

## Comparative study of *K*-shell exciton series in condensed neon and nitrogen by electron time-of-flight spectroscopy

B. Kassühlke, P. Averkamp, S. Frigo, and P. Feulner

*Physikdepartment E20, Technische Universität München, 85747 Garching, Germany*

W. Berthold

*Max-Planck-Institut für Quantenoptik, 85748 Garching, Germany*

(Received 25 October 1996)

Photon absorption and electron emission phenomena in the near-*K*-edge region are studied for condensed neon and nitrogen, employing electron time-of-flight spectroscopy in combination with high photon-energy resolution. Surface and bulk ionization thresholds and bulk exciton excitation energies, including the  $1s^{-1}5p$  transition, are reported for neon multilayers. For condensed nitrogen, we observe three different types of resonant features in the near-*K*-edge region. Type 1, which is excited by photon energies less than the surface N  $1s$  ionization potential, is clearly of excitonic nature. Resonances of type two are seen for excitation energies which are larger than the surface *K* edge by more than 3 eV. They parallel maxima seen in the kinetic-energy distribution of secondary electrons and can be well explained by transitions into regions of the conduction band with a high density of states. Peaks of the third category appear between the surface *K* edge and 1.5 eV above. They have no analogs either in the secondary electron distribution, or in the amplitude of the N  $1s$  photoemission signal. We explain them as bulk excitons converging toward the bottom of the conduction band of solid nitrogen. In our study, we demonstrate that electron time-of-flight spectroscopy is a versatile analytical tool for the study of electronic properties of samples such as those which suffer severely under beam induced damage and charging. [S0163-1829(97)09815-9]

### INTRODUCTION

Even for simple molecular solids like condensed nitrogen, data on exciton series are comparatively rare. Outer- and inner-shell excitons, which in the isolated molecule correspond to excited states with *valence* character (that is, those involving promotion of electrons into empty *valence* orbitals), give rise to narrow lines with well-resolved vibrational fine structure.<sup>1-7</sup> They are only marginally shifted in energy compared with their counterparts in the gas phase,<sup>1,2,5-9</sup> although the oscillator strength may differ markedly.<sup>3</sup> Excitons which correspond to *Rydberg* excitations in the free molecule involve a final state that is composed of wave functions of higher principal quantum numbers than the valence orbitals. In the solid, they generally lead to broad lines which are difficult to detect.<sup>1-4,10</sup> Particularly in solid nitrogen, outer-shell excitons derived from *Rydberg* states appear only as very broad maxima in high-resolution electron-energy-loss spectroscopy,<sup>1</sup> optical spectroscopy,<sup>2</sup> momentum-transfer spectroscopy,<sup>3</sup> and photon-stimulated desorption (PSD) of neutral molecules.<sup>4</sup> Even the perturbation of the vibrational spacing of valence states, with which they interfere, and which is strong in the isolated molecule, vanishes (see Ref. 2, and references therein). However, in order to achieve an understanding of screening and electron correlation effects in these molecular solids, data on the energetic shifts of exciton energies and series limits encountered upon solidification are necessary, despite these spectroscopic difficulties. This need has been convincingly shown by the ample experimental and theoretical work devoted to excitons in rare gas solids (see, e.g., Ref. 11 and references therein).

In previous experiments on condensed neon<sup>12</sup> and

nitrogen,<sup>6,7</sup> we showed that PSD in particular is a powerful tool for the investigation of surface excitations. However, our previous studies on nitrogen were lacking in the ability to unambiguously detect series limits inside the bulk and on the surface,<sup>6,7</sup> which is necessary for a clear discrimination between photoabsorption maxima due to bound-exciton states on one hand, and continuum resonances due to regions with high density of states of the conduction band on the other. To address these topics, we have employed electron time-of-flight (TOF) spectroscopy which can answer these questions readily. As in our previous studies, we use inner *K*-shell excitation; because of the localized, atomic nature of the core hole and because of its simple electronic symmetry, the interpretation of the results is simplified.

Electron TOF spectroscopy has demonstrated its outstanding capabilities, namely, high sensitivity combined with good energy resolution (particularly for low-energy electrons), in many gas-phase studies. Apart from experiments with laser excitation, little use has been made of this principle for the investigation of *solid* samples.<sup>13</sup> We show that such an instrument is a sensitive and versatile tool for synchrotron studies of solids and surfaces. It is especially useful for spectroscopy of insulating samples like molecular and rare-gas solids, which suffer severe and rapid beam damage due to charging and photon-stimulated desorption and/or dissociation. The TOF instrument design is straightforward, and the energy dependence of its transmission function can easily be calculated. The TOF technique not only allows the pinpointing of ionization thresholds, but also provides exciton excitation and binding energies as well as data on electron affinities. Comparing excitation, photoelectron, and secondary electron spectra from multilayers of neon and nitrogen

for the excitation of *K* electrons to Rydberg-like orbitals, we obtain surprising results on the kinetic-energy distribution of secondary electrons, particularly for solid nitrogen. We show that the width of the exciton and/or Rydberg series differs considerably for the bulk, the surface of the solid, and the gas phase, and that the electron affinity of solid nitrogen might be more negative than hitherto expected.<sup>14</sup>

## EXPERIMENT

All data have been obtained utilizing the PM-5 (previously denoted HE-PGM-III) monochromator at BESSY, Berlin, during single-bunch operation of the storage ring. The spectral resolution of the monochromator was better than 100 meV (250 meV) at the *K* edges of nitrogen (neon). For all experiments reported here, we have employed a TOF spectrometer designed especially for the investigation of solid samples. It can be used for the detection of electrons, ions, and metastable particles.<sup>15</sup> It consists of a plane entrance grid of at least 85% transparency, a field-free drift tube of variable length (5–23.5 cm), and two microchannel plates (MCP's). The latter are mounted in a chevron arrangement as detector. The whole detector assembly is optimized for a small skew time. All spectra reported here were taken with a maximum flight path of 23.5 cm.<sup>16</sup> The sample was positioned parallel to the entrance grid at a distance of 2 mm. The entrance grid, the inner part of the drift tube, and the entrance grid of the MCP detector were covered with graphite for work-function homogeneity. Between the sample and the entrance grid we applied an accelerating voltage to ensure that threshold electrons starting with zero kinetic energy at the sample reached the MCP detector just before the advent of the next light pulse in order to avoid ambiguities due to the overlap of signals from different periods of electron bunches in the storage ring. At BESSY, their repetition rate is about 4.8 MHz, and depending upon the current in the storage ring, the bunch length is 300–500 ps.

We took great care to minimize the distortion of the electron trajectories through stray magnetic fields. The drift tube itself was shielded by three layers of annealed  $\mu$  metal. The magnetic field, particularly on the short acceleration path between the sample and the entrance grid, was further reduced by employing three pairs of large area, square Helmholtz coils mounted outside the UHV chamber. To set the currents of these coils correctly, we used three UHV-compatible, bakeable flux-gate sensors,<sup>15</sup> which were mutually perpendicularly oriented to each other. These magnetic sensors were placed close to the sample position by means of a mechanical feedthrough; in combination with the Helmholtz coils, they enabled the compensation of the environmental magnetic field of about 80  $\mu$ T to less than 0.1% of its initial value.

Very efficient data acquisition was accomplished by using electronics based on integrated high-speed counters and field programmable logic gate arrays (FPGA's).<sup>15</sup> Four counters serve as clocks for the arrival times of up to four independent particles per light pulse (256 channels). After one cycle, the data are transferred to a multichannel analyzer constructed from FPGA devices. After accumulating one TOF spectrum at a distinct photon energy, which typically took 3 s for  $1.4 \times 10^7$  acquisition cycles, the data were transferred to a

computer and arranged in three dimensional sets (see below); the monochromator was then moved to the next photon-energy position, and the above procedure was repeated. Apart from the preamplifier and the discriminator, the whole device exclusively employs digital electronics, featuring shadow times (the minimum spacing of two events necessary for discrimination), and dead times (the time between two acquisition periods required for data handling, counter resetting, etc.) as short as 1.5 and 9 ns, respectively, and maximum count rates up to 20 MHz. With our design, we obtained the correct scale for the kinetic energy without any free parameters (see below).

The UHV chamber housing the analyzer (base pressure better than  $3 \times 10^{-9}$  Pa) allowed independent setting of the angles of polarization (surface normal  $\mathbf{n}$  against  $\mathbf{E}$  vector of the light) and detection ( $\mathbf{n}$  against detector axis) by simultaneously rotating the detector chamber and the sample manipulator. For enhanced surface sensitivity, grazing incidence of the synchrotron light by  $7^\circ$  with respect to the surface was used.<sup>6</sup> The samples were prepared by dosing reproducible amounts of neon and nitrogen (purity better than 99.99%) onto a Ru(001) crystal serving as substrate that was cooled to either less than 7 K (for neon), or 20 K (for nitrogen). We determined the thickness of the layers from thermal-desorption spectra (TDS) by comparing monolayer and multilayer peaks. Before dosing, the substrate was cleaned by sputtering with argon ions and repeated heating and cooling in  $10^{-4}$  Pa of oxygen. The oxygen was removed from the surface by flashing to 1570 K, and the cleanliness of the surface was checked by near-edge x-ray-absorption fine-structure performed with the TOF analyzer, by x-ray photoemission spectroscopy (XPS) (utilizing a laboratory Al  $K\alpha$  source in combination with a hemispherical electron-energy analyzer), and by using well-known features of xenon thermal-desorption spectroscopy as fingerprints for the absence of impurities.<sup>17</sup> This was done in order to avoid any sample contaminations or spatial work-function inhomogeneities due to impurities adsorbed at the interface.

## RESULTS AND INTERPRETATION

### Neon multilayers

Our strategy is as follows: We first display *K*-shell excitation results for solid neon, using them to introduce the features and potential of our technique. We then compare these to data obtained for *K*-shell excitation of nitrogen multilayers, displaying and discussing only results on nitrogen core excitons which are related to Rydberg-like transitions. (A TOF study of the  $\pi$  resonance, whose vibrational structure allows, via saturation effects, a detailed investigation of electron transport, will be published elsewhere.<sup>18</sup>) From this, interesting results on the excitonic or ionic nature of distinct resonances can be derived.

Figure 1 displays a pseudo-three-dimensional electron distribution spectrum for the *K*-shell region of neon for films  $\approx 40$  layers thick. It is the sum of four identical scans obtained from different samples, each of which is composed of 300 individual electron kinetic-energy spectra. The primary TOF spectra were recorded in sequence, incrementing the photon energy by 33 meV before each scan. We transformed the TOF data to the kinetic-energy representation by multi-

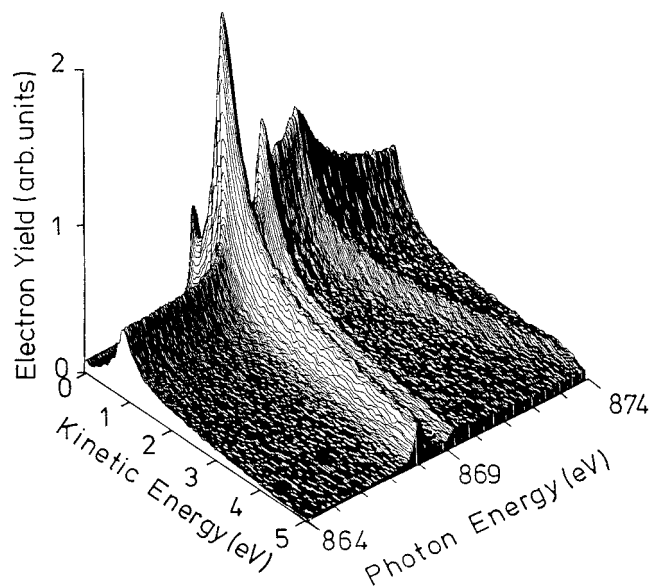


FIG. 1. Pseudo-three-dimensional electron spectrum obtained from neon film of 40 layers ( $864 \text{ eV} \leq h\nu \leq 874 \text{ eV}$ ,  $0 \text{ eV} \leq E_{\text{kin}} \leq 5 \text{ eV}$ ).

plying (a) with a Jacobian converting the density of states from the time to the energy domain, and (b) with a kinetic-energy-dependent factor. The latter accounts for the variation of the angle of acceptance with the electron energy, according to the plate capacitor geometry between sample and entrance grid. Finally, we changed the axis intervals. For the calibration of the kinetic-energy scale, we used the channel location of the x-ray fluorescence signal corresponding to infinite kinetic energy,<sup>19</sup> and the steep cutoff at zero kinetic energy corresponding to electrons from the vacuum level. By considering the geometry of the detector and the applied voltages, the kinetic-energy scale was then calculated without any further fit parameters. We note that the shape and width of the cutoff at zero kinetic energy reflects the energy resolution of the analyzer as well as the quality of the sample. For clean samples with a homogeneous work function and an optimum setting of the Helmholtz coils (see above), we obtained cutoffs that were less than 30 meV wide, and which appeared at constant zero kinetic energy (in the raw data, at constant TOF) for the whole photon-energy scan. Any charging, or contamination which affects the work function, shifted and broadened this cutoff, thus enabling a very sensitive *in situ* monitor of charging. We note that the complete set of spectra included in Fig. 1 has been recorded with a total dose of only  $10^{11}$  photons.

Focusing on the details of Fig. 1, we find a maximum at 1-eV *kinetic energy*, which is visible at all photon energies, and peaks at 868.3- and 869.5-eV *photon energy*, which are visible at all kinetic energies between zero and the maximum energy of decay electrons around 820 eV. (In Fig. 1, we display only the low-energy range, because it is of most interest for our purpose.) Also, neon  $1s$  photoemission shows up as a feature with a slope of unity (i.e., constant binding energy); it is discussed below.

The maxima at constant *excitation energy* are due to the  $1s^{-1}3p$  and  $1s^{-1}4p$  inner-shell excitons.<sup>12,20,21</sup> The maxima at constant *kinetic energy* are due to a high density of elec-

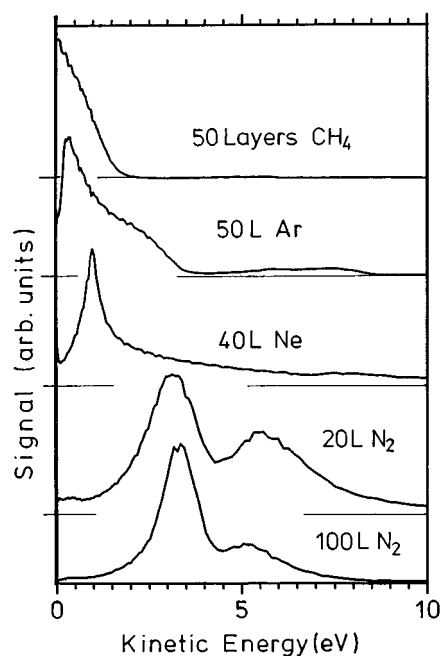


FIG. 2. Secondary-electron energy distributions from (top to bottom) 50 layers methane, 50 layers argon, 40 layers neon, 20 layers nitrogen, and 100 layers nitrogen.

tronic states; the peak at 1 eV in Fig. 1 corresponds to the bottom of the conduction band, which for solid neon lies above the vacuum level (see below). This is best seen from the traces in Fig. 2, where we display kinetic-energy distributions of secondary electrons that have been obtained by integrating over the photon energy for methane, argon, neon, and nitrogen. For the light rare gases neon and argon, which are known to exhibit negative electron affinity,<sup>11</sup> narrow maxima appear at 1 and 0.3 eV, respectively, above the vacuum level. These are due to secondary electrons that have been cooled to the bottom of the conduction band. Whereas for argon our data are in perfect agreement with previous results, for neon we obtain a value for the electron affinity which is 0.3 eV closer to the vacuum level than the literature value of 1.3 eV (see references in Ref. 11). The emission between zero kinetic energy and these maxima must be due to emission from the surface of the film, either by primary photon excitation of surface atoms or by inelastic scattering processes into surface states. This is corroborated by the ratio between the amplitudes at the peak and at the vacuum level becoming larger as the multilayer becomes thicker (see the discussion for nitrogen multilayers). For condensed nitrogen, the energy distribution of the secondaries peaks at even higher kinetic energy, i.e., the majority of electrons ejected are extremely hot, whereas for, e.g., solid methane the maximum lies at the vacuum level, clearly indicating the absence of negative electron affinity for this material (Fig. 2).

Traditional total-electron yield data can easily be obtained from the TOF data by integrating over the total range of kinetic electron energy, or for partial yield only over the energy range where autoionization and Auger emission appears. A similar procedure is applied here, but for a different energy region. For a further investigation of the electronic excitations, we cut the data in Fig. 1 parallel to the photon-energy axis at a kinetic energy of  $1.00 \pm 0.04 \text{ eV}$ , i.e., at the

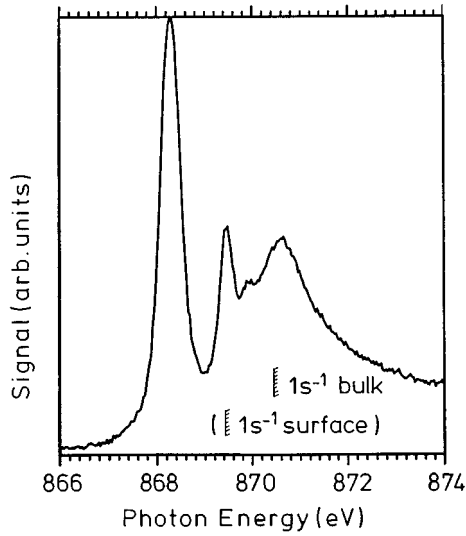


FIG. 3. Excitation spectrum obtained from data of Fig. 1 by cutting at constant  $E_{\text{kin}}=1$  eV. The positions of the bulk and surface *K* edges are indicated.

bottom of the conduction band. The result is depicted in Fig. 3. Apart from the two excitons already mentioned, we see a third peak at 869.9 eV due to the  $1s^{-1}5p$  transition, and a broad maximum centered around 870.6 eV which we assign to the neon  $1s^{-1}$  threshold electrons. Due to post-collision interaction (PCI), core ionization threshold peaks are broadened, and the ionization potential corresponds to the onset rather than to the maximum of the peak.<sup>22</sup> The onset of the threshold electron distribution is observed at 870.2 eV for 1-eV kinetic energy, corresponding to threshold electrons with respect to the bottom of the conduction band, and at 869.3 eV for  $E_{\text{kin}}=0$  eV, corresponding to the ionization threshold for surface atoms. The spacing of 0.9 eV between the onset of surface and bulk emission is slightly smaller than the electron affinity of 1 eV. This might reflect a less effective polarization screening of the core hole at the surface due to the incomplete shell of next neighbors as compared with the bulk.

The difference of the Ne  $1s$  and  $2s$  binding energies from XPS is 821.5 eV.<sup>23</sup> From Ne  $2s$  threshold spectra, which exhibit much narrower peaks than those for Ne  $1s$  because of a longer lifetime and much weaker PCI effects, we obtain 48.9 eV for the inner ionization threshold.<sup>24</sup> By adding the above difference, we arrive at a Ne  $1s$  bulk threshold of 870.4 eV. In summary, we find that the inner *K*-shell ionization threshold of solid neon is equal or slightly larger than that of 870.3 eV for neon gas, whereas the value for the surface is lower, the spacing between surface and bulk threshold being the electron affinity or 0.1 eV less (see the compilation in Table I).

We further note that apart from the  $5p$  resonance, which hitherto could only be resolved in the gas phase (see, e.g., Refs. 26 and 27), our bulk exciton data are in perfect agreement with our PSD study,<sup>12</sup> a photoabsorption study by Hiraya *et al.*,<sup>20</sup> and results from free neon clusters.<sup>21</sup> Comparing our exciton binding energies of 2.1, 0.9, and 0.5 eV with those of 3.0, 1.42, and 0.85 eV for the gas phase (Table I), we find an overall energy-level compression for the solid. For the *surface* excitons, whose excitation energies are accessible with PSD,<sup>12</sup> this compression is even stronger, squeezing the energy difference between  $1s^{-1}3p$  and  $1s^{-1}$  to less than 1.8 eV (Table I). This compression is due to differential energy shifts arising from competition between polarization screening and short-range repulsion, which in different manners influence the excitonic and ionic states. This has been discussed in detail in Ref. 12, and we refrain from repeating those arguments here.

Surprisingly, the individual exciton peaks become narrower as the principal quantum number  $n$  becomes larger. The full width at half maximum (FWHM) for  $1s^{-1}3p$  is more than 0.5 eV, whereas for  $1s^{-1}4p$  and  $1s^{-1}5p$  it is about 0.35 eV (Fig. 3). This certainly is not due to a strongly reduced lifetime of the core hole for  $n=3$ ; participant decay channels are very weak for rare gases, as for all neutral core excitations with Rydberg character.<sup>29</sup> The decay rate of the  $1s$  hole should not strongly depend on the nature of the initial core-excited state, therefore. Moreover, such a selective broadening of the  $1s^{-1}3p$  excitation is not seen for the gas phase.<sup>26,27</sup> We believe that we also can exclude line

TABLE I. Excitation ( $E_{\text{ex}}$ ) and exciton binding energies ( $E_b$ ) for the neon *K* edge. Data marked a, b, c, and d are taken from Refs. 26–28, and 12, respectively (Ref. 25). The binding energies of the surface excitons (in brackets) are calculated with the ionization potential of the  $1s$  orbital referred to the vacuum level.

Sample	Polarization		Energetics of neon <i>K</i> -shell excitations (eV)				
			$1s^{-1}3s$	$1s^{-1}3p$	$1s^{-1}4p$	$1s^{-1}5p$	$1s^{-1}$
Gas phase		$E_{\text{ex}}$	865.1 <sup>a</sup>	867.1 <sup>a,b</sup>	868.68 <sup>a,b</sup>	869.25 <sup>a,b</sup>	870.1 <sup>a</sup> , 870.27 <sup>c</sup>
		$E_b$	5.0	3.0	1.42	0.85	
Surface	$A_z$	$E_{\text{ex}}$	865.6 <sup>d</sup>	867.6 <sup>d</sup>	868.8 <sup>d</sup>		869.4±0.2
		$E_b$	(3.8)	(1.8)	(0.6)		
	$A_{xy}$	$E_{\text{ex}}$		867.8 <sup>d</sup>	868.6 <sup>d</sup>		
		$E_b$		(1.6)	(0.8)		
Bulk		$E_{\text{ex}}$		868.3±0.1	869.5±0.1	869.9±0.1	870.4±0.2
		$E_b$		2.1	0.9	0.5	

broadening by saturation. In photoabsorption, the degree of saturation depends on the optical density of the absorbing layer. In a surface experiment, this quantity is related to the sampling depth of the utilized probes,<sup>18</sup> which in our case are electrons. We obtain identical widths of the  $1s^{-1}3p$  line for secondary electrons of 1 eV, and for decay electrons of more than 600 eV, although their escape depth is certainly not identical. Moreover, peak fitting shows that the broadening of the  $1s^{-1}3p$  line is of the Gaussian type whereas saturation would induced Lorentzian-like broadening.<sup>18</sup> The only other possibility is that the excitation energy suffers inhomogeneous line broadening by the solid environment. Such a selective line broadening upon condensation has previously also been observed for the neon  $2s^{-1}np$  excitons,<sup>23,30,31</sup> whereas the lines of  $2p^{-1}ns$  excitons are comparatively narrow [a FWHM less than 200 meV (Ref. 32)]. Contrary to the latter, which are delocalized excitations, the  $1s$ , and probably also the  $2s$ , excitons are of the Frenkel type. These are located at one single atom, and, following Ref. 33, we can treat them as an impurity. It has been shown that lattice vibrations cause Gaussian line broadening for such localized excitations (see Ref. 33 and references therein). The amount of broadening depends on the temperature (and the zero-point motion, which for solid neon cannot be neglected<sup>34</sup>), and the variation of the potential with the distance from the nearest neighbors. Our data clearly show that the line broadening is maximum for the  $3p$  wave function, which is spatially least extended. From PSD results we know that the surface-to-bulk shifts, as well as the polarization shifts, are of comparable size for the  $3p$  and  $4p$  excitons (Table I). Obviously, long-range variations of the environment, like the solid-vacuum interface, which affect the whole wave function independent of the quantum number, induce energy shifts of similar magnitude (their sign, however, may differ<sup>12</sup>). The situation might be different if we consider short-range variations, e.g., phonons of high momentum, that cause anticorrelated movements of neighboring atoms. The spatially extended wave function of the exciton with larger principal quantum number would then average over many unit cells and be less influenced. Temperature-dependent experiments, which were beyond the scope of our apparatus, could help to solve this question.

### Nitrogen multilayers

We now turn to the main topic of this study, namely, excitons in nitrogen multilayers. Pseudo-three-dimensional photon- and kinetic-energy spectra from nitrogen multilayers for excitation around the  $K$  edge and above are depicted in Figs. 4(a) and 4(b), where different aspects of the same spectrum are emphasized. Polarization effects are of minor importance (see below). Particularly for larger electron kinetic energies, polarization-dependent differences vanish, and we display data only for  $A_{xy}$  light in Fig. 4(a) (for details of the notation, refer to the figure captions). In the energy distribution of electrons, two strong maxima are visible at about 3.1 and 5.5 eV for all photon energies. The exact position of these maxima depends slightly upon the layer thickness. For thin films (20 layers) we find 3.1 and 5.5 eV, and for very thick films (100 layers) 3.25 and 5.15 eV (see Figs. 4 and 2). For thicker films, the maximum at 3.25 eV becomes more

dominant, whereas emission at 5.15 eV and at the vacuum level decreases. (For convenience, we neglect the small thickness-dependent shifts, and denote the peaks with the numbers 3.1 and 5.5 as obtained from thin layers.) Clearly, most electrons are emitted with kinetic energies much larger than zero. The total electron yield excitation spectrum, obtained from Fig. 4 by integrating over all electron energies, exhibits several resonances labeled  $A$  through  $G$  for photon energies of 406.8, 407.3, 408.4, 409.4, 410.3, 412.2, and 415 eV [Fig. 5(b), for  $A_z$  and  $A_{xy}$  light]. Some of these resonances appear also as excitonlike structures at constant photon energy in Fig. 4(a), i.e., parallel to the kinetic-energy axis. Polarization effects are negligible [Fig. 5(b)].

Next we focus on the N  $1s$  photoemission feature clearly visible in Fig. 4. From a two-dimensional contour plot (not shown) of the data from Fig. 4, we obtain  $408.85 \pm 0.15$  eV for the ionization threshold. This is about 1 eV less than for the gas phase,<sup>9</sup> and in good agreement with values of 409.1 and 409.4 eV, respectively, obtained for dimers<sup>35</sup> and nitrogen clusters of mixed size.<sup>36</sup> The intensity of the N  $1s$  photoemission, however, encounters considerable modulation, depending on the excess kinetic energy. This is evident when one inspects the high-kinetic-energy side of the two maxima at 3.1- and 5.5-eV electron energy, where N  $1s$  emission is strong [Fig. 4(a)]. On top of the maxima the emission is resonantly enhanced, whereas it becomes very weak on the low-energy side of the 3.1-eV peak [Fig. 4(b)]. In particular, no enhancement is visible when crossing the excitation feature  $E$  or when approaching  $D$ , for either polarization. In Fig. 5 the photoabsorption of nitrogen gas [Fig. 5(a); from Ref. 9], our total electron yield [Fig. 5(b)], and the kinetic-energy distribution of secondary electrons from Fig. 2 is shown [Fig. 5(c)], differentially shifted so that the vacuum level coincides for all of them. The gas-phase spectrum exhibits resonances due to N  $1s$  to Rydberg transitions between 406 eV and the  $K$  edge, a maximum with vibrational fine structure between 414 and 415 eV explained as  $\pi$ - $\pi$  shake-up accompanying the  $\pi$  resonance at 401 eV, and the  $\sigma$  resonance near 420 eV.<sup>9,37-39</sup> We note that aligning the excitation spectra for gaseous and solid nitrogen at the vacuum level probably is incorrect for the shake-up feature. As a pure valence excitation, it suffers little energy shift from condensation and should be aligned at the  $\pi$  resonance, which is nearly unshifted upon condensation,<sup>5-7</sup> or cluster formation.<sup>36</sup>

Comparing all traces, we can draw conclusions on the nature of maxima  $A$ – $G$ . Feature  $F$  corresponds exactly with the low-energy peak of the electron distribution at 3.1 eV. It has no counterpart in the gas phase, and therefore must be a pure solid-state effect. The resonant enhancement of the photoemission yield clearly identifies it as due to a regime of high density of states, i.e., to the structure of the conduction band. Feature  $G$  not only contains contributions from band structure, but also from the shake-up processes known in the gas phase [compare Figs. 5(a) and 5(b)]. Maxima  $A$ – $C$  are below the vacuum level, and must be due to bound excitations. Peaks  $D$  and  $E$ , however, lie clearly above it, even though they are absent in the secondary electron yield [Fig. 5(c)], as well as in the gas-phase photoabsorption [Fig. 5(a)]. They can neither be easily explained as due to band-structure features, nor to transitions existing in the isolated molecule,

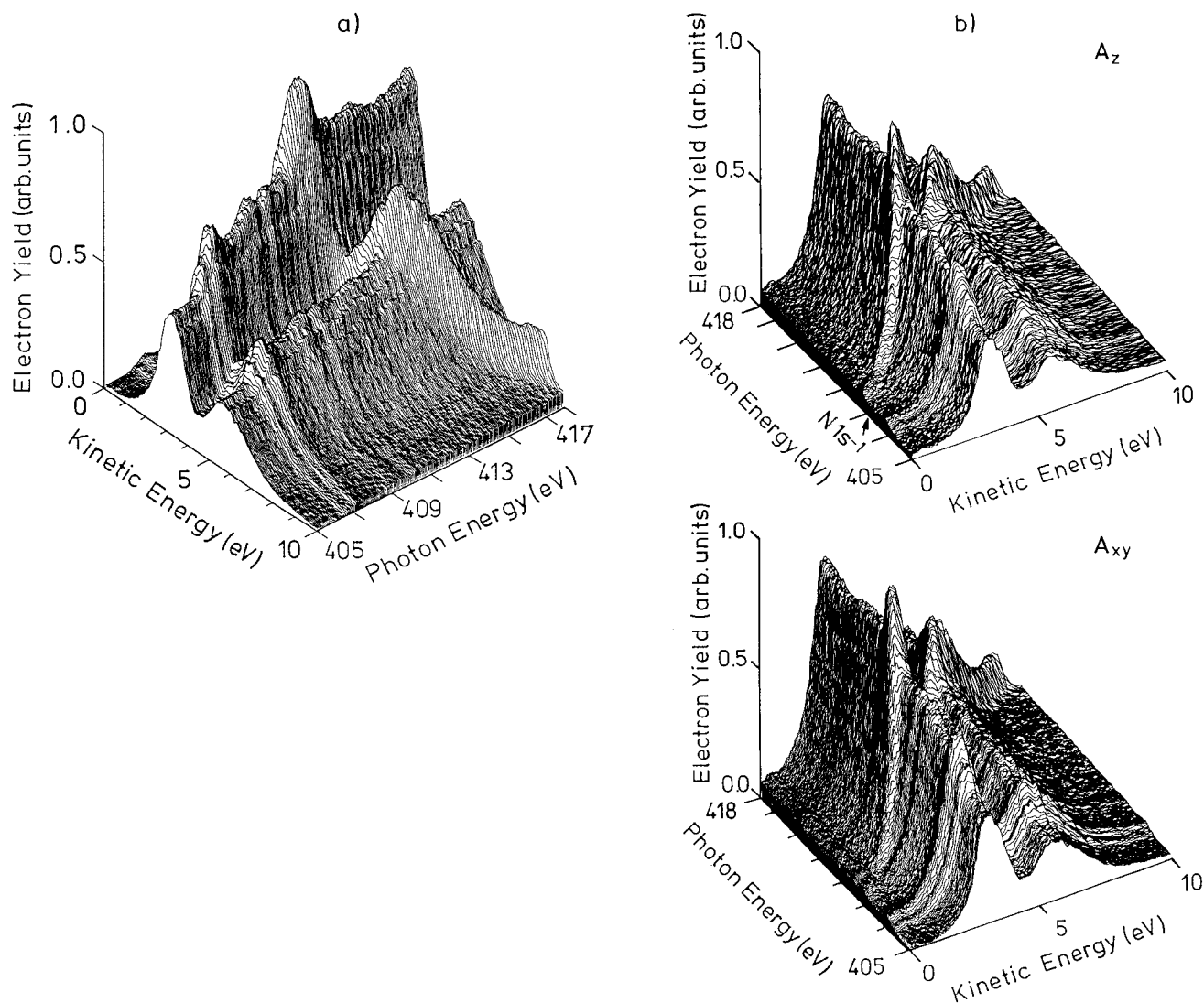


FIG. 4. Pseudo-three-dimensional electron spectrum obtained from 20 layers of nitrogen ( $405 \text{ eV} \leq h\nu \leq 418 \text{ eV}$ ;  $0 \text{ eV} \leq E_{\text{kin}} \leq 10 \text{ eV}$ ), viewed (a) from high and (b) from low  $E_{\text{kin}}$ . (Polarization as indicated;  $A_z$ :  $\mathbf{E}$  vector almost parallel to surface normal  $\mathbf{n}$  (the tilt angle is  $7^\circ$ );  $A_{xy}$ :  $\mathbf{E}$  perpendicular to  $\mathbf{n}$ .) The position of the surface  $K$  edge is indicated by an arrow in (b) ( $A_z$ ).

at least not as due to one-electron transitions (see below). Comparing with the results from solid neon, and with UPS data from solid nitrogen,<sup>40</sup> it would be tempting to assign  $D$  and  $E$  as bound excitations, and the prominent feature in the secondary electron distribution at 3.1 eV to the lowest conduction band in solid nitrogen, toward which they converge.

We point out that the electron states of an exciton and the conduction bands are derived from the same atomic or molecular orbital, the only difference being the presence or the absence of a positive hole, which pulls the electron states to lower energy with respect to the vacuum level. For inner-shell holes, which are well localized, the situation is particularly simple. In this view, the maximum energetic range over which an exciton series extends is a direct measure for the binding energy encountered by the lowest unoccupied level upon switching on the hole interaction. For solid neon the lowest conduction bands are derived from the  $n=3$  atomic orbitals. For the neutral atom, these wave functions are very extended, giving rise to large widths of the conduction bands

[the  $W_{2\gamma}-\Gamma_1$  separation of the lowest conduction band is as large as 9.2 eV (Ref. 41)]. Comparing the electron affinities of  $-0.3$  eV for the isolated atom,<sup>42</sup> and  $-1$  eV for the solid (our value), we find a shift of  $-0.7$  eV which reflects short-range repulsion due to electron correlation. The total width of the neon  $1s^{-1}$  exciton series is about 4 eV if we include the  $1s^{-1}3s$  surface excitation (the latter is dipole forbidden in the bulk<sup>12</sup>).

For nitrogen, the situation is more complicated, because unfilled orbitals with dominant valence as well as dominant Rydberg character exist. The lowest empty molecular orbital is the  $1\pi_g$  orbital which is derived from  $2p_{x,y}$  functions of the nitrogen atoms; in the absence of an inner- or outer-shell hole, it shows up as a negative-ion resonance at 2.3 eV above  $E_v$  in the gas phase.<sup>43</sup> Promotion of a  $1s$  electron to this orbital gives rise to the  $\pi$  resonance. In solid nitrogen, it shows vibrational fine structure like the gas.<sup>5-7,9</sup> The vibrational energies are very close to the gas-phase values,<sup>9,18</sup> and the experimentally obtained blueshift of 140 meV for the

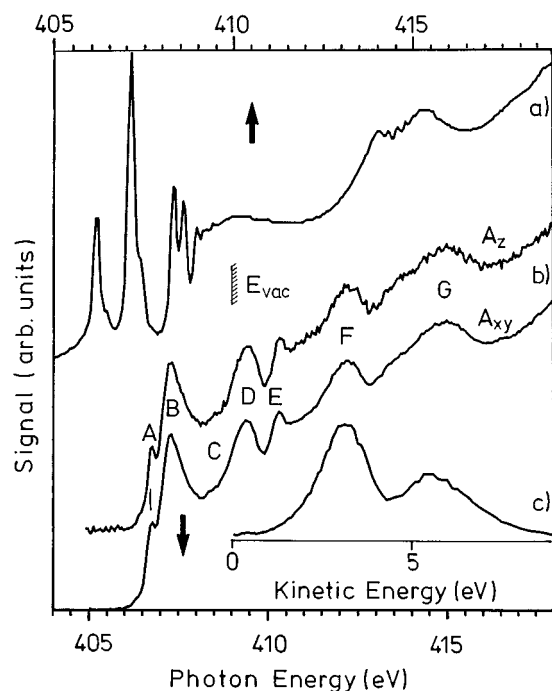


FIG. 5. A comparison of (a) the photoabsorption in the gas phase (Ref. 9), and (b) the total electron yield from the solid (for  $A_z$  and  $A_{xy}$  light), with (c) the energy distribution of secondary electrons obtained from the solid. The spectra are aligned at the vacuum level.

$0 \rightarrow 0$  transition<sup>6</sup> is not far from the calibration error. This reflects the pure valence character of this orbital. Following the suggestion in Ref. 40, we assign the feature seen at 3.1 eV in the secondaries to a conduction band derived from that  $1\pi_g$  state. We note that the photon energy spacing between the  $\pi$  resonance and the 3.1-eV final state is about 11 eV, huge compared with the energetic width of exciton series in solid neon and also the Rydberg series in nitrogen gas [Fig. 5(a)]. It reflects the much stronger interaction of the narrow  $2p$  wave functions with the inner-shell hole. It stays constant upon condensation, indicating minor interaction of the orbitals with the environment. Coming back to the nature of the maxima  $D$  and  $E$  in the excitation spectra, we conclude that they clearly would have to be explained as core excitons if this  $1\pi_g$ -derived conduction band were the lowest. The electron affinity of solid nitrogen would then be 3.1 eV (or about 1 eV less if we take the onset and not the maximum of this resonance). The exciton features of solid nitrogen (now neglecting the  $\pi$  resonance because of its valence character) would essentially be composed of two contributions, namely, members of a surface and a bulk series. The small, narrow peaks  $A$  and  $C$  below the vacuum level, as well as parts of peak  $B$ , which in PSD show polarization dependent behavior,<sup>6,7</sup> certainly belong to the surface series; maxima  $D$ ,  $E$ , and the rest of  $B$  then would be bulk features. (The division of  $B$  into bulk and surface parts may look rather arbitrary. We base this tentative interpretation on the finding that in PSD maximum  $B$  is smaller with respect to  $A$ , and slightly narrower than obtained here.<sup>6,7</sup>) Without calculation, the correlation of these structures with the Rydberg maxima in the gas phase cannot be solved; however, we expect ordering according to the principal quantum number.

We believe that we also can exclude the possibility that the maxima  $E$  and  $D$  are due to two-electron excitations. For nitrogen gas, the existence of two transitions with  $\pi$  and  $\sigma$  symmetry ( $1\sigma_u^{-1}1\pi_u^{-1}1\pi_g^2$  and  $1\sigma_u^{-1}3\sigma_g^{-1}1\pi_g^2$ ) 9.47 and 10.48 eV above the  $\pi$  resonance has been predicted by calculations of Arneberg *et al.*<sup>37</sup> Recently, a distinct feature at 384 eV in electronic decay spectra appearing at excitation energies between 408.6 and 412.3 eV has been explained as their signature.<sup>39</sup> These excitations are valence transitions, and, following the above argumentation, we expect minimal condensation shifts, i.e., we expect them in the solid for the energy range where the maxima  $E$  and  $D$  are observed. We can, however, clearly rule out that  $E$  and  $D$  are due to these transitions because of two reasons. First, the experimentally obtained range of excitation energies for these multielectron transitions does not coincide with our data. It extends 2 eV beyond peak  $E$ . Second, maxima  $D$ , and in particular  $E$  with a FWHM of less than 1 eV, are much too narrow to be explained by excitations involving promotion of two electrons into the antibonding  $1\pi_g$  orbital. These multielectron excitations have been shown by electronic decay spectroscopy<sup>39</sup> and (for the isoelectronic molecule CO) by PSD (Refs. 44 and 45) to be strongly antibonding, leading to (ultra-)fast dissociation. In a recent ion-PSD investigation under high-photon-energy-resolution conditions, we obtained about 5 eV for the width of the  $1\pi^{-1}2\pi$  shake-up to the  $\pi$  resonance in chemisorbed CO,<sup>45</sup> which should correspond to the  $1\pi_u^{-1}1\pi_g$  shake-up in nitrogen (compare Refs. 37 and 46). We conclude that electron emission due to these two-electron excitations certainly contributes to the smooth background seen in our spectra in this energy range, but clearly cannot be responsible for distinct narrow peaks.

An alternative explanation of our data would be that the  $1\pi_g$  band is not the lowest, and that one or more additional bands exist which then would have to be derived from orbitals of higher quantum number, e.g., those states giving (in the presence of a core hole) rise to the Rydberg excitations seen in the gas phase, and in the solid below the surface  $K$  edge. They should induce very similar features as observed for the rare-gas solids neon and argon. Because vibronic coupling is much weaker for Rydberg than for valence states, we expect the density-of-state (DOS) maxima related to them to be narrower than the broad maximum at 3.1 eV. Maxima  $D$  and  $E$  could then be due to inner free-electron-hole excitations. However, we would have to explain why these hypothetical bands do not show up either in the secondary-electron yield or in the N  $1s$  photoemission signal, for either polarization. If such a band existed, hot electrons should be cooled to its bottom as it is seen for the rare gases (Fig. 2). This cooling should be more effective for nitrogen because of the larger number of inelastic channels that are available, including optical phonons, rotational excitation, and internal vibrations of the molecules as opposed to the rare-gas solids, where emission of acoustic phonons is the only loss mechanism.

Comparing secondary-electron emission from thin and thick nitrogen layers, we indeed find an indication of cooling. The emission at the 5.5-eV maximum, which must be due to a higher conduction band, is decreased for the thicker film (Fig. 2). However, emission of electrons with energies below 2 eV is decreased as well. One could argue that a band

gap around 2.5 eV could effectively hinder relaxation, but even then we would expect to see these bands as areas of high amplitude in the  $N\ 1s$  photoemission yield; this is clearly not the case [Fig. 4(b)]. We believe that we also can exclude the possibility that such bands would be invisible in our data because of lack of a DOS projected onto the surface of our films. Our samples, in particular the thick ones, are certainly polycrystalline and exhibit surfaces of different orientation, which in combination with the different polarization conditions that have been employed should rule out any suppression of electron emission due to accidental involvement of symmetry-selection rules.

In conclusion, we find that the first explanation is much more likely than the second. Our preferred explanation of the maxima *D* and *E* as bound excitations is in perfect agreement with the UPS results from Lau, Fock, and Koch.<sup>40</sup> Our conclusions are, however, in some contradiction to low electron transmission data of Bader *et al.*, who find only  $-0.8$  eV for the electron affinity of solid nitrogen.<sup>14</sup> We hope that future band-structure calculations which are in preparation<sup>47</sup> will clarify the situation.

### SUMMARY

In summary, we have shown that electron TOF spectroscopy is a very useful tool for the investigation of the elec-

tronic properties of solid insulators. It easily and unambiguously provides data on outer ionization thresholds, kinetic energy distributions of secondary electrons, excitation energies of excitons, and resonances in the photoemission yield. From these primary results, conclusions on the electron transport, the density of states in the conduction band, and inner ionization potentials and the electron affinity can be drawn. Comparing *K*-edge excitation phenomena for the Rydberg region of solid neon and nitrogen, for nitrogen we find strong evidence of the existence of bound, excitonlike states more than 1 eV above the outer ionization threshold, indicating a vanishing density of states of conduction bands in this energy region.

### ACKNOWLEDGMENTS

Valuable discussions with M. Lindroos, D. Menzel, and W. Wurth are gratefully acknowledged. We thank N. Heckmair and the staff of BESSY (in particular, C. Hellwig, C. Jung, and H. Pfau) for help during the experiments, and M. Glanz for producing a portion of the electronics. One of us (S.F.) thanks the Humboldt Foundation for support. The work was supported by the Deutsche Forschungsgemeinschaft through Project No. Me 266/21-1, and through Sonderforschungsbereich 338 C13.

- 
- <sup>1</sup>R. M. Marsolais, M. Michaud, and L. Sanche, *Phys. Rev. A* **35**, 607 (1987).
- <sup>2</sup>E. Boursey and J.-Y. Roncin, *Phys. Rev. Lett.* **26**, 308 (1971), and references therein.
- <sup>3</sup>C. Tarrío and S. E. Schnatterly, *Phys. Rev. Lett.* **66**, 644 (1991).
- <sup>4</sup>P. Wiethoff, R. Scheuerer, and P. Feulner (unpublished).
- <sup>5</sup>D. Arvanitis, H. Rabus, M. Domke, A. Puschmann, G. Comelli, H. Petersen, L. Tröger, T. Lederer, G. Kaindl, and K. Baberschke, *Appl. Phys. A* **49**, 393 (1989).
- <sup>6</sup>R. Scheuerer, Ph.D. thesis, Technische Universität München, 1996.
- <sup>7</sup>P. Feulner, R. Scheuerer, M. Scheuer, G. Remmers, W. Wurth, and D. Menzel, *Appl. Phys. A* **55**, 478 (1992).
- <sup>8</sup>W. F. Chan, G. Cooper, R. N. S. Sodhi, and C. E. Brion, *Chem. Phys.* **170**, 81 (1993).
- <sup>9</sup>C. T. Chen, Y. Ma, and F. Sette, *Phys. Rev. A* **40**, 6737 (1989).
- <sup>10</sup>R. Scheuerer, P. Feulner, P. Wiethoff, W. Wurth, and D. Menzel, *J. Electron Spectrosc. Relat. Phenom.* **75**, 161 (1995).
- <sup>11</sup>See, e.g., N. Schwentner, E.-E. Koch, and J. Jortner, *Electronic Excitations in Condensed Rare Gases*, Springer Tracts in Modern Physics Vol. 107 (Springer, Berlin, 1985).
- <sup>12</sup>P. Wiethoff, H.-U. Ehrke, B. Kassühlke, C. Keller, W. Wurth, D. Menzel, and P. Feulner, *Phys. Rev. B* **55**, 9387 (1997).
- <sup>13</sup>A. S. Aleksandrovsky and V. V. Slabko, *J. Electron Spectrosc. Relat. Phenom.* **74**, 149 (1995).
- <sup>14</sup>G. Bader, G. Perluzzo, L. G. Caron, and L. Sanche, *Phys. Rev. B* **30**, 78 (1984).
- <sup>15</sup>B. Kassühlke, diploma thesis, Technische Universität München, 1994 (unpublished).
- <sup>16</sup>We note that shorter distances between the entrance grid and the detector increase the sensitivity and the energy resolution for threshold electrons, but deteriorate the performance for higher kinetic energies.
- <sup>17</sup>H. Schlichting and D. Menzel, *Surf. Sci.* **272**, 27 (1992).
- <sup>18</sup>B. Kassühlke and P. Feulner (unpublished).
- <sup>19</sup>The fluorescence yield was measured with the microchannel plates by blocking the analyzer to electrons of any energy by applying a suitable potential to the sample.
- <sup>20</sup>A. Hiraya, K. Fukui, P.-K. Tseng, T. Murata, and M. Watanabe, *J. Phys. Soc. Jpn.* **60**, 1824 (1991).
- <sup>21</sup>F. Federmann, O. Björneholm, A. Beutler, and T. Möller, *Phys. Rev. Lett.* **73**, 1549 (1994).
- <sup>22</sup>A. Niehaus, *J. Phys. B* **10**, 1845 (1977).
- <sup>23</sup>P. Wiethoff, Ph.D. thesis, Technische Universität München, 1995.
- <sup>24</sup>The auxiliary neon  $2s$  data were measured with the TOF device at the TGM-1 monochromator at BESSY.
- <sup>25</sup>References 26 and 27 give identical values for the Rydberg excitation energies in neon gas. However, the value for the *K* edge of Ref. 26 is lower by about 0.2 eV than that of Ref. 28 which has been obtained with great experimental efforts. Although the latter may be closer to reality, we have used the value of Ref. 26 for the calculation of the binding energies, because we expect minimum relative errors if both quantities are determined by the same experiment.
- <sup>26</sup>A. P. Hitchcock and C. E. Brion, *J. Phys. B* **13**, 3269 (1980).
- <sup>27</sup>J.-E. Rubensson, M. Neeb, A. Bringer, M. Biermann, and W. Eberhardt, *Chem. Phys. Lett.* **257**, 447 (1996).
- <sup>28</sup>L. J. Saethre, T. D. Thomas, and L. Ungier, *J. Electron Spectrosc. Relat. Phenom.* **33**, 381 (1984).
- <sup>29</sup>W. Wurth and D. Menzel, in *Application of Synchrotron Radiation to High Resolution Studies of Molecules and Molecular Adsorbates on Solids*, edited by W. Eberhardt, Springer Series in

- Surface Science Vol. 35 (Springer, Berlin, 1995), p. 171.
- <sup>30</sup>P. Wiethoff, H.-U. Ehrke, D. Menzel, and P. Feulner, *Phys. Rev. Lett.* **74**, 3792 (1995).
- <sup>31</sup>R. Haensel, G. Keitel, C. Kunz, and P. Schreiber, *Phys. Rev. Lett.* **25**, 208 (1970).
- <sup>32</sup>V. Saile and E. E. Koch, *Phys. Rev. B* **20**, 784 (1979).
- <sup>33</sup>G. Zimmerer, in *Excited State Spectroscopy in Solids*, edited by U. M. Grassano and N. Terzi (Societa' Italiana di Fisica, Bologna, 1987), p. 36.
- <sup>34</sup>I. F. Silvera, *Rev. Mod. Phys.* **52**, 393 (1980).
- <sup>35</sup>C. Y. Ng, *Adv. Chem. Phys.* **52**, 263 (1983).
- <sup>36</sup>E. Rühl, A. P. Hitchcock, P. Morin, and M. Lavollée, *J. Chim. Phys.* **92**, 521 (1995).
- <sup>37</sup>R. Arneberg, H. Ågren, J. Müller, and R. Manne, *Chem. Phys. Lett.* **91**, 362 (1982).
- <sup>38</sup>E. Shigemasa, K. Ueda, Y. Sato, T. Sasaki, and A. Yagishita, *Phys. Rev. A* **45**, 2915 (1992); Kaidee Lee, Dae Young Kim, Chien-I Ma, and D. M. Hanson, *J. Chem. Phys.* **100**, 8550 (1994).
- <sup>39</sup>M. Neeb, A. Kivimäki, B. Kempgens, H. M. Köppe, J. Feldhaus, and A. M. Bradshaw, *Phys. Rev. Lett.* **76**, 2250 (1996).
- <sup>40</sup>H.-J. Lau, J.-H. Fock, and E. E. Koch, *Chem. Phys. Lett.* **89**, 281 (1982).
- <sup>41</sup>See, e.g., N. C. Bacalis, D. A. Papaconstantopoulos, and W. E. Pickett, *Phys. Rev. B* **38**, 6218 (1988).
- <sup>42</sup>R. J. Zollweg, *J. Chem. Phys.* **50**, 4251 (1969).
- <sup>43</sup>G. J. Schulz, *Rev. Mod. Phys.* **45**, 423 (1973).
- <sup>44</sup>R. Treichler, W. Riedl, W. Wurth, P. Feulner, and D. Menzel, *Phys. Rev. Lett.* **54**, 462 (1985).
- <sup>45</sup>S. Frigo, P. Feulner, B. Kassühlke, C. Keller, and D. Menzel (unpublished).
- <sup>46</sup>H. Ågren and R. Arneberg, *Phys. Scr.* **30**, 55 (1984).
- <sup>47</sup>M. Lindroos *et al.* (unpublished).